Applied Catalysis B: Environmental 343 (2024) 123556

Contents lists available at ScienceDirect

Applied Catalysis B: Environmental

journal homepage: www.elsevier.com/locate/apcatb

Mechanistic insight into the destruction of perfluoroalkyl acids on gallium oxide

Junyao Wu [a,b], Yu Mao [b], Shan Yi [a], Sudip Ray [a,c], Wei Gao [a,*], Ziyun Wang [b,*]

[a] Department of Chemical and Materials Engineering, University of Auckland, Auckland 1142, New Zealand
[b] School of Chemical Sciences, University of Auckland, Auckland 1010, New Zealand
[c] New Zealand Institute for Minerals to Materials Research, 100 Mackay Street, Greymouth 7805, New Zealand

ARTICLE INFO

Keywords:
PFAS
Density functional theory
Photocatalysis
Mineralization mechanism
Defluorination

ABSTRACT

Per- and polyfluoroalkyl substances (PFAS) are a large group of persistent, toxic, and highly water-soluble chemicals resulting from human activities, and their pervasive presence in the environment has garnered global concern. Although accelerating the deconstruction of PFAS is of urgent importance, it still lacks a fundamental understanding of the PFAS mineralization mechanism in photocatalysis. Here, we apply the density functional theory (DFT) calculations to assess the thermodynamic favorability of all possible reaction pathways for two ultrashort perfluoroalkyl acid model compounds (i.e., $CF_3CF_2COO^-$ and $CF_3CF_2SO_3^-$) on β-Ga_2O_3 surfaces. Our results show that the optimal mineralization pathway includes defluorination and defunctionalization, shortening of the carbon chain, and the mineralization of C_1 species, which computationally rationalized many experimental observations of PFAS destruction. This work provides pivotal quantum-level insights into the comprehensive and crucial reaction mechanisms for PFAS degradation, which will facilitate the design of effective catalysts for PFAS mineralization.

1. Introduction

Per- and polyfluoroalkyl substances (PFAS) are products of the modern chemical industry and have been widely incorporated into industrial and consumer products [1]. These compounds are characterized by their distinct structure, including at least one fully fluorinated methyl (-CF_3) or methylene carbon (-CF_2) group [2]. The intrinsic chemical stability of the carbon-fluorine bond (C–F, 531.5 kJ mol^{-1}) enables PFAS to have high environmental persistence and resistance to degradation, resulting in their ubiquitous presence in the environment, such as drinking water, food, and air, and bioaccumulation in both aquatic and terrestrial species [3]. The toxicological results indicate that long-term PFAS exposure can pose adverse health effects to public health, possibly inducing organ damage, suppressed immunity, hormonal and reproductive problems, and cancer [4]. It has raised increasing global attention on PFAS contamination over time.

Throughout the lifecycle of PFAS, including production, usage, and disposal, perfluorocarboxylic acids (PFCAs, $C_nF_{2n+1}COOH$) and perfluorosulfonic acids (PFSAs, $C_nF_{2n+1}SO_3H$), have emerged as the predominant PFAS contaminants due to their direct application in commercial products and accumulation as terminal transformation products of other PFAS [5]. Apart from separation methods, technologies like electrochemical oxidation [6–8], plasma treatment [9,10], and thermal processes [11,12] have been developing to treat PFAS with different chain lengths, playing a crucial role in PFAS remediation [13,14]. Among these technologies, heterogeneous photocatalysis offers a promising solution for PFAS degradation, which provides simultaneous or alternation oxidative (h^+) and reductive (e^-) conditions to decompose PFAS into smaller molecules under mild conditions [15,16]. Extensive research was conducted to explore the intrinsic catalytic activity of photocatalysts, including their ability to enhance light absorption and prolong the lifetime of charge carriers [17–24]. However, the atomic-level degradation mechanism remains elusive, hindering further research for effective PFAS destruction.

Depending on the reaction conditions, two major mechanisms of PFAS destruction have been proposed: reductive destruction and oxidative destruction. During reductive reaction processes, hydrated electrons (e^-_{aq}) are the effective reducing agent to attack the resistant C-F bond. Previous studies have proposed two parallel degradation pathways for PFAS owing to e^-_{aq}, including H/F exchange and chain-shortening processes [25,26]. Due to the cleavage of C-F bonds and elimination of F, followed by adding H atoms, the H/F exchange

* Corresponding authors.
E-mail addresses: w.gao@auckland.ac.nz (W. Gao), ziyun.wang@auckland.ac.nz (Z. Wang).

https://doi.org/10.1016/j.apcatb.2023.123556
Received 14 August 2023; Received in revised form 27 October 2023; Accepted 22 November 2023
Available online 25 November 2023

produces less fluorinated organic radical anions.

Several possible approaches were proposed for the chain-shortening pathway. One pathway consists the stepwise -CH_2- removal through two H/F exchanges, leading C-C bond breakage [25]. Another is called the decarboxylation-hydroxylation-elimination-hydrolysis (DHEH) mechanism, which also occurs in the oxidation regime [26–28]. In addition to measuring intermediates and reactive species experimentally to confirm the degradation mechanisms, theoretical computations such as density functional theory (DFT) or molecular dynamics (MD) calculations have been used to explore the mechanisms of how hydrated electrons accelerate PFAS degradation at the atomic level [29,30].

Researchers through adding an excess electron/charge in the PFAS molecule, or simulating electrons being polarized by surrounding water and losing sufficient energy to become sub-stable localized species bound with water to approximate the actual hydrated electrons. Both calculation methods show that although the α C-F bonds of PFOA ($C_nF_{2n+1}COOH$, n = 7) and PFOS ($C_nF_{2n+1}SO_3H$, n = 7) are thermodynamically more reactive, all other C-F bonds are likely to dissociate. The C-F bond in the middle position of the carbon chain can also be the reactive region [28,30].

On the other hand, researchers have investigated the oxidative degradation mechanism of PFAS. It is widely believed that the oxidative photocatalyst systems produce active oxidants such as h^+,·OH, HOO·, $^1O_2$, or $O_2^{\cdot-}$ which are involved in the reactions during the photoinduced process [14,31]. Despite several reaction routes that have been proposed in combination with the detected main degradation intermediates and quantum mechanical simulations, the degradation mechanisms remain contentious. In the initial reaction stages, two possible reactions have been proposed in literature: direct defunctionalization (losing a carboxyl or sulfur trioxide group to release CO_2 or SO_3) and F-elimination from the original PFAS anion [14,20]. However, the current experimental and computational results cannot conclude which mechanism is more favorable [20]. There were also different views on the carbon chain-shortening pathway.

In the previous study, based on the detection of PFAS and perfluoroalkyl (C_nF_{2n+1}) with different chain lengths, researchers proposed a chain-shortening mechanism for single-carbon-chain shortening process undergoing the hydroxylation, elimination, and hydrolysis after defunctionalization (also known as the DHEH process) [15,31,32]. Each PFAS is successively shortened in this process by removing α-position CF_2 during each cycle. Another single-carbon shortening mechanism assumes that the shorter-chain PFAS was obtained through the progressive elimination of CF_2 group [33]. Evidence also suggests that PFAS destruction can occur through mechanisms other than non-single carbon shortening [34]. Furthermore, while nearly complete defluorination has been detected experimentally in some photocatalytic systems [31,35], the mineralization of F-containing radicals, such as CF_2, CF_3, and CFO, remains rarely explored in the literature.

Despite the aforementioned efforts, a few questions must be answered: (I) In the initial degradation stage, how do defluorination and defunctionalization proceed? (II) What is the most energetically favorable pathway of chain shortening from C_2 to C_1 species? (III) What is the pathway of the defluorination and mineralization of C_1 species? (IV) Are the defluorination, chain-shortening, and mineralization in the photooxidation and photoreduction conditions integrated into a universal theory to fully depict the PFAS degradation. This work systematically investigates the degradation pathways of ultrashort-chain perfluoroalkyl acids (PFAAs) over β-Ga_2O_3 via theoretical approaches using DFT calculations. These ultrashort-chain compounds, including perfluoropropanoic acid (PFPrA, C_2F_5COOH) and perfluoroethane sulfonic acid (PFEtS, $C_2F_5SO_3H$), are the minimum repeat unit of PFAAs. We analyzed the thermodynamic feasibility of each presumed reaction step and proved DHEH mechanism is the most likely mineralization route to explain the phenomenon of previous literature. This work also provides a deeper understanding of PFAS degradation mechanisms for the development of technically sound PFAS removal techniques.

2. Computational details

All DFT calculations were conducted using the Vienna ab initio simulation package (VASP 5.4.4) [36,37]. The Perdew-Burke-Ernzerhof (PBE) functional within generalized gradient approximation (GGA) was utilized to describe the electron interaction [38]. At the same time, the project-augmented wave (PAW) method was used to treat the core–electron interaction [38,39]. The electron wave functions were expanded in the plane waves with a kinetic energy cutoff of 450 eV. The Methfessel-Paxton (MP) method with a smearing width of 0.20 eV was adopted for the transition metal surfaces and interfaces [40]. A (3 × 3 × 1) *k*-point mesh sampling was performed for the electronic self-consistent calculations. The convergence criteria for the energy and force were set to 10^{-5} eV and 0.05 eV $Å^{-1}$, respectively. The DFT-D3 method was used to account for van der Waals corrections. Literature suggests that compared to other oxide systems, such as TiO_2 (E_g = ~ 3.2 eV), ZnO (E_g = ~ 3.3 eV), and In_2O_3 (E_g = ~ 2.8 eV), the β-Ga_2O_3 system exhibits stronger redox capabilities and higher PFAS destruction performance due to its wider bandgap (~ 4.9 eV) [41,42]. The low-index facets of β-Ga_2O_3 (001), (100), (010), and (201) were selected (Fig. 1), causing the commercially synthesized β-Ga_2O_3 to consist of these facets mainly and were widely studied [43]. A vacuum layer of 15 Å along the Z direction was set to avoid the imagined interaction between slabs. The optimized lattice parameters of slabs were shown in Table S1. All slabs were composed of six layers, of which the lower half layers were fixed. In contrast, the upper half layers were relaxed.

We assumed that the reaction steps in PFAS degradation included dehydrogenation, defunctionalization, defluorination, oxygenation, and C-C bonding breakage consistent with previous works [30,31,44]. When calculating the reaction energy, the energies (*E*) of isolated F and O atoms were adopted as the energy difference in HF and half hydrogen ($E_{HF} - \frac{1}{2}E_{H_2}$), H_2O, and hydrogen ($E_{H_2O} - E_{H_2}$) molecules, respectively. The reaction energy (ΔE, in units of eV) was used to evaluate the thermodynamic feasibility of certain reaction pathways. The effect of the entropy of adsorbate and adsorption sites is small enough to be neglected in the calculations for ΔG.

3. Results and discussion

3.1. Overview of the whole reaction network

We first built the reaction networks with possible pathways, including three main stages: the initial stage, C_2 stage (32 C_2 species), and C_1 stage (10 C_1 species), as displayed in Fig. 2. In the initial stage, we found that the parent PFPrA and PFEtS undergo hydrogen dissociation spontaneously according to DFT calculations. It can be hypothesized that dehydrogenation can be the first step before degradation. Afterward, we evaluated the possibilities of defunctionalization and defluorination processes of α-position and β-position carbon.

In the second and third stages, we investigated the mineralization pathway from perfluoroalkyl radical (CF_3CF_2·) to CO_2. All possible intermediates ($C_xF_yO_z$, $x \leq 2$, $y \leq 5$, $z \leq 2$) were considered and then optimized using DFT calculations. Based on the computational results, we discerned unstable intermediates that occur with dissociation or reconstruction from all potential intermediates, which were removed from the potential intermediate candidate [45]. 32 C_2 species in Fig. 2 (b) and 10 C_1 species in Fig. 2(c) were considered for further study. In Fig. 2(b), the C_2 species in each circle can be converted into species in the same position of the adjacent circle through defluorination. In addition, the C_1 species in Fig. 2(c) can be generated from C_2 species in Fig. 2(b) through C-C scission, and C_1 species can be further oxidized into CO_2. In such reaction networks (Fig. 2b and c), all intermediates can be interconverted through oxygenation (red arrows) or defluorination (green arrows) steps. It can be observed that multiple pathways of the formation or elimination of each intermediate are present. Furthermore,

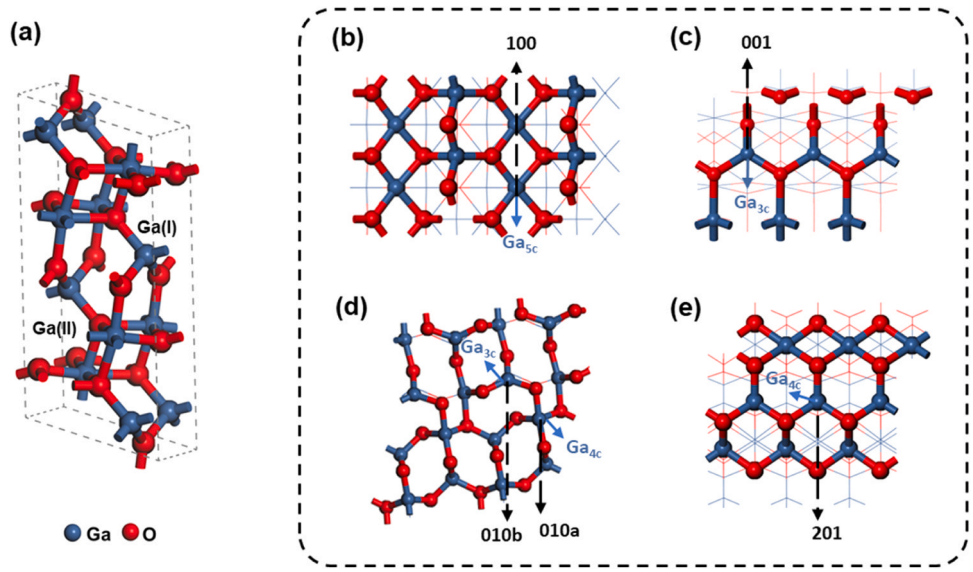

Fig. 1. (a) Models of β-Ga_2O_3 crystal structure. Top views of (b) (100), (c) (001), (d) (010), and (e) (201) facets of β-Ga_2O_3. The atoms on the surface and sub-surfaces are represented in the ball-and-stick model and the rest are shown in the line model.

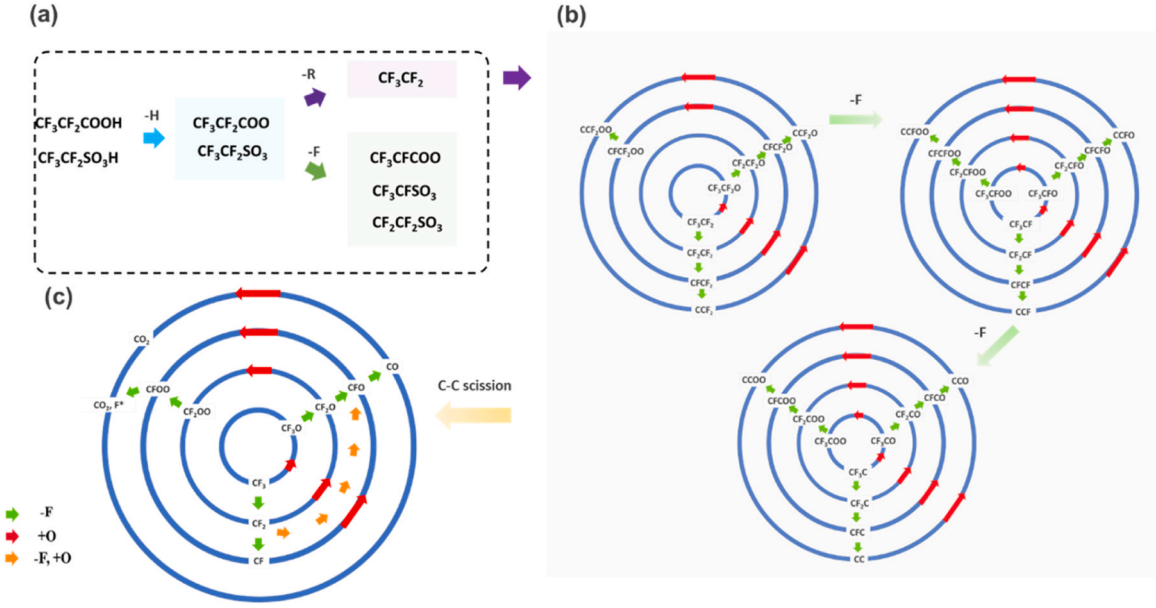

Fig. 2. A schematic of the reaction network: (a) pathways for the initial reaction, (b) pathways for C_2 species, and (c) pathways for C_1 species.

we calculated all intermediates in the reaction network in Fig. 2(b) and (c) on *β*-Ga_2O_3(100), (001), (010), and (201) facets and investigated the reaction energy changes along all possible reaction pathways.

3.2. Stage I: dehydrogenation, defunctionalization/defluorination

We calculated the hydrogen dissociation reactions of PFCAs (C_3) and PFSAs (C_2) on the preceding β-Ga_2O_3 surfaces. The hydrogen dissociated spontaneously from PFSAs (C_2) and was captured by neighboring oxygen atoms when PFSAs (C_2) adsorbing at Ga sites (Fig. 3c and d). We performed transition state calculations to better describe the dehydrogenation process (Fig. S6 (a) and (b)). The results showed that the energy barriers of PFCA (C_3) and PFSA (C_2) were 1.57 eV and 1.55 eV on (010) facet, respectively. Contrary to this observation, the dehydrogenation process does not act as the rate-determining step for PFAS degradation. PFAS predominantly exist in their anionic form rather than in their acidic states under the given experimental parameters [46]. Compared to PFCAs (C_3), PFSAs (C_2) was more easily dehydrogenated on all β-Ga_2O_3 surfaces (Fig. 3a), consistent with the lower *pKa* value of perfluoroalkyl sulfonic acid [47]. In addition, the dehydrogenation energies of both PFCAs (C_3) and PFSAs (C_2) are in a sequence: (010b) > (001) > (201) > (010a) > (100).

Results of previous studies suggested that both fluorine loss and defunctionalization mechanisms for the initial step of PFSAs/PFCAs degradation reaction could occur [31]. We conducted a comparison of the -R reaction energies of PFCAs (C_3) and PFSAs (C_2) on various facets (Fig. 3b). PFCAs (C_3) is more prone to chain-shortening reactions by defunctionalization than PFSAs (C_2), which coincides well with prior literature [48–51]. This points to that PFCAs are more susceptible to degradation than PFSAs. Within the β-Ga_2O_3 system, PFSAs (C_2) exhibited various defunctionalization activities highly related to the surface status followed the order of (001) > (100) > (010b) > (010a)

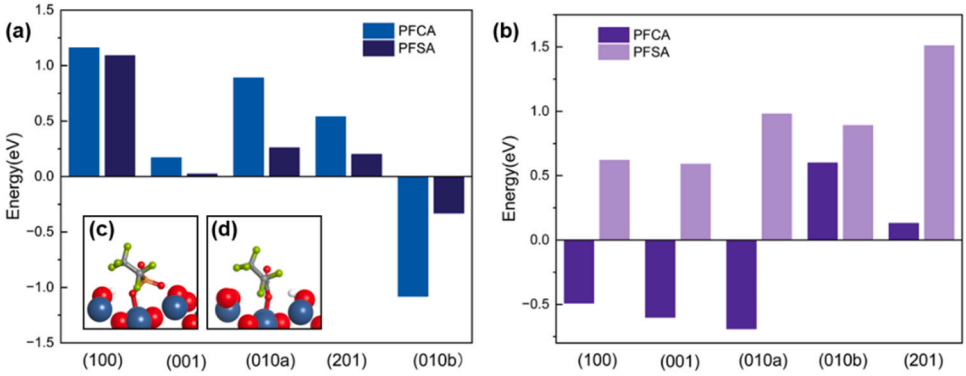

Fig. 3. (a) Dehydrogenation energies and (b) defunctionalization energies of PFSAs (carbon number = 2) and PFCAs (carbon number = 3) on five β-Ga_2O_3 surfaces. The inset is the schematic of dehydrogenation of PFCAs/PFSAs (c) co-adsorbed *$CF_3CF_2SO_3$ and *H atom of PFSAs (C_2) and (d) co-adsorbed CF_3CF_2COO and H atom of PFCAs (C_3) on β-Ga_2O_3(100) surface. The white, gray, red, green, and indigo balls represent H, C, O, F, and Ga atoms, respectively. This notation is used throughout the paper.

> (201) (Step S4, Table 1). For PFCAs (C_3), it followed the order of (010a) > (001) > (100) > (201) > (010b) (Step C3, Table 1). Among tested facets, removal of the carboxylic functional head of PFPrA can exothermically occur on (100), (001), and (010a).

Our theoretical calculations have yielded insights into the thermodynamic feasibility of the defluorination of ultra-short chain PFAS at the atomic level (Table 1). Fluorine loss on α-position carbon is the preferred pathway for PFCAs (C_3) and PFSAs (C_2) compared to defluorination on other positions. For the α-C defluorination reaction of PFCAs (C_3) and PFSAs (C_2), the activities of β-Ga_2O_3 facets follow the order of (001) (0.58 eV) > (010b) (0.90 eV) > (010a) (2.27 eV) and (001) (0.96 eV) > (010b) (1.85 eV) > (010a) (2.50 eV), respectively. This finding agrees with prior experimental and computational studies that lower C-F dissociation energy on the α-position carbon enables defluorination at this position more favorably [16,28,52,53].

Overall, the defunctionalization shows a lower energy upshift on all facets, suggesting a more facile process. The adsorption of PFCAs (C_3) and PFSAs (C_2) on the β-Ga_2O_3(001) surface is illustrated in Fig. 4 5 for the occurrence of -F and -R reactions.

3.3. Stage II: reaction pathway of C_2 species to C_1 species

Previous photocatalytic experiments involving PFAS studied the reactive species, including holes (h^+), electrons (e^-), superoxide radicals ($O_2^{\bullet-}$), and hydroxyl radicals (•OH) [31]. The •OH is potentially produced by h^+ and water molecules, and e^- reacts with oxygen to generate $O_2^{\bullet-}$ [20]. Previous photocatalytic studies support the significant role of •OH on perfluoroalkyl radicals (defluorination reaction products) [32,54]. Here, we analyze the reactions of hydroxyl radicals with the defunctionalized product *CF_3CF_2. The oxygenation step (+O) energy was calculated for the energy of H_2O and H_2.

Upon exploring the subsequent reactions of perfluoroalkyl radicals, we considered four cases: C-C cleavage to produce CF_3 and CF_2, α-position C defluorination to yield CF_3CF, β-position C defluorination to yield CF_2CF_2, and oxygen addition to form CF_3CF_2O. Our calculated results reveal that direct C-C cleavage is more difficult than α-C defluorination, β-C defluorination, and oxygenation. For all surfaces, β-C defluorination is more favorable than α-C defluorination, possibly due to the relatively better stability of the CF_2CF_2 product. Furthermore, our results exhibit that the oxygen addition step forming CF_3CF_2O has a negative reaction energy change across every site. In contrast to the thermodynamic infeasibility of C-C cleavage and defluorination, the oxygenation reaction is thermodynamically feasible at all sites except (100). Therefore, the formation of CF_3CF_2O is the more probable step in this reaction.

We calculated the proposed DHEH pathway, reported in various PFAS degradation systems, such as photochemical, photocatalytic, electrocatalytic, and electron beam degradation of straight-chain PFAAs [15,31,55]. PFAS degradation pathways have closely followed the DHEH degradation route whenever a perfluoroalkyl fragment can be generated, especially the complex PFAS molecular [31,56]. We calculated the energy change of elementary step in the DHEH mechanism on β-Ga_2O_3 surface. In particular, the process from CF_3CFO to CF_3COO involves a two-step reaction. Fig. 6a shows that in pathway I, direct +O of CF_3CFO to CF_3CFOO is challenging to achieve, except for the possible reaction occurring at the (201) plane, possible because of the saturation of CF_3CFO ligand. CF_3CFOO appears to be more feasible to defluorinated upon the occurrence of the +O reaction, decreasing the reaction energy to below − 2 eV on all surfaces. Conversely, the process of C-C breakage for CF_3COO to form CF_3 and CO_2 displays a high energy upshift exceeding 3.5 eV, suggesting this is a low likelihood reaction.

Pathway II favors CF_3CFO first defluorination over oxygenation on all sites. The energy change of the reaction to generate CF_3CO followed by CF_3COO is less than 0 eV, enabling the reaction to proceed. Pathway II has a less-energy increase for converting CF_3COO to CF_3 and CO_2 compared to Pathway I, suggesting the priority. We further discussed the reaction energy change of the total reaction from *CF_3CF_2 to *CF_3 (Fig. 6a). It can be found that cleaving CF_3COO to CF_3 and CO_2 exhibits the highest energy upshift, indicating that CF_3COO is the process and a rate-determining step. For the (001) and (010a) surfaces, the release of CF_3COO is difficult and comparable to its converting to CF_3 and CO_2. The activities of $CF_3COO \rightarrow CF_3 + CO_2$ on different planes follow the order of: 010a (0.83 eV) > 100 (1.29 eV) > 201 (1.40 eV) > 010b

Table 1
The reaction energy changes of dehydrogenation, defunctionalization, and defluorination steps on β-Ga_2O_3(100), (001), (010), and (201) facets.

Step *i*	Reaction elementary step	Reaction energy changes (eV)				
		(100)	(001)	(010a)	(010b)	(201)
S1	* + $CF_3CF_2SO_3H$ → $CF_3CF_2SO_3$* + H	1.09	0.02	0.26	-0.33	0.20
S2	$CF_3CF_2SO_3$* → CF_3CFSO_3* + F	-	0.58	2.27	0.90	-
S3	$CF_3CF_2SO_3$* → $CF_2CF_2SO_3$* + F	-	1.28	2.07	1.90	-
S4	$CF_3CF_2SO_3$* + H_2O → CF_3CF_2* + H_2SO_4	0.62	0.59	0.98	0.89	1.51
C1	* + CF_3CF_2COOH → CF_3CF_2COO* + H	1.16	0.17	0.89	-1.08	0.54
C2	CF_3CF_2COO* → CF_3CFCOO* + F	-	0.96	2.50	1.85	-
C3	CF_3CF_2COO* → CF_3CF_2* + CO_2	-0.49	-0.60	-0.69	0.60	0.13

Note: " - " means the optimized structure is unstable.

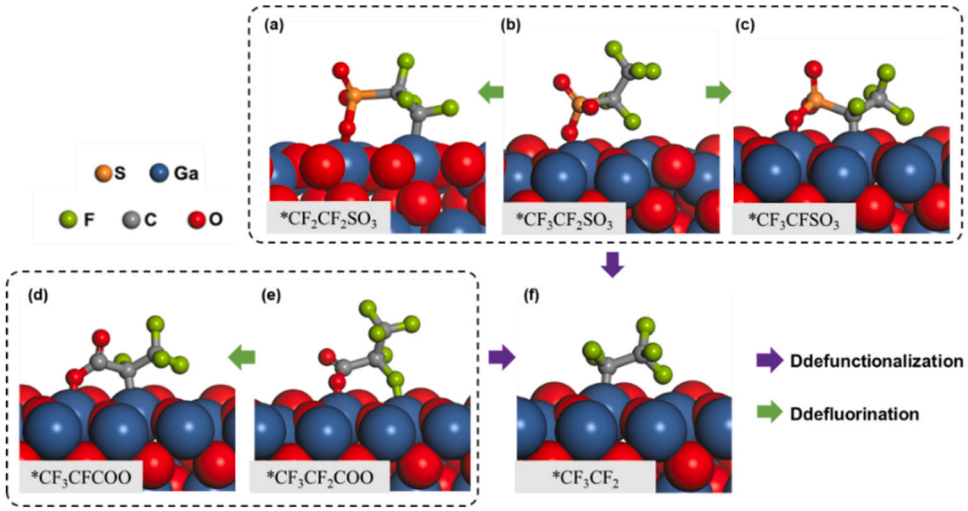

Fig. 4. Models along the reaction pathway for: (a) $*CF_2CF_2SO_3$, (b) $*CF_3CF_2SO_3$, (c) $*CF_3CFSO_3$, (d) $*CF_3CFCOO$, (e) $*CF_3CF_2COO$, and (f) $*CF_3CF_2$ on β-Ga_2O_3(001).

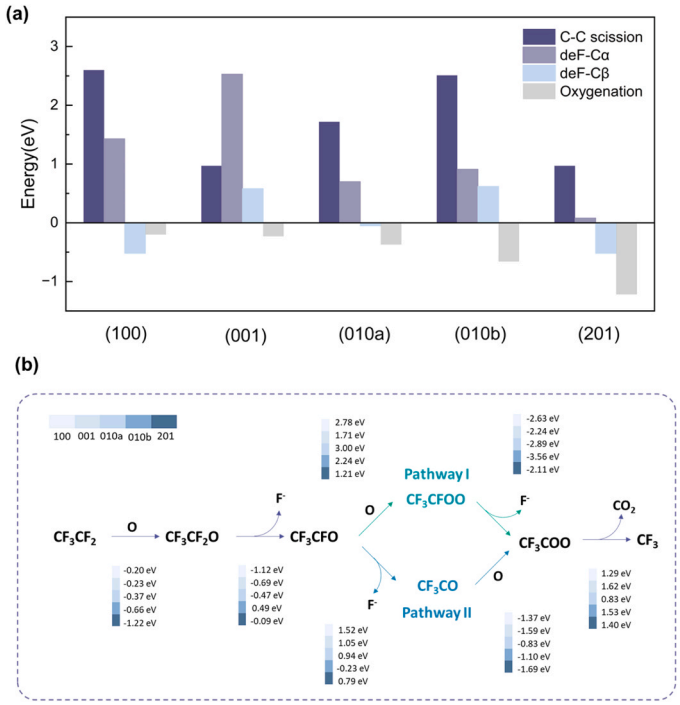

Fig. 5. (a) The reaction energy of C-C scission, α-C defluorination, β-C defluorination, and oxygenation reactions of CF_3CF_2 at various β-Ga_2O_3 surfaces. (b) Reaction networks and reaction energy changes of the DHEH pathways at various β-Ga_2O_3 surfaces. (α-C or Cα refers to the first carbon atom adjacent to the functional group of CF_3CF_2-R. β-C or Cβ refers to the second carbon atom next to the functional group of CF_3CF_2-R. This notation is used throughout the paper.).

(1.53 eV) > 001(1.62 eV).

We have investigated the energy change for breaking the C-C bond of various significant C_2 intermediates to form C_1 metabolites (Fig. 6b). Results indicate that CF_3CFOO (all sites), CF_3CO (all sites), and CF_3CF_2O (excluding site (010a)) are the main C_2 intermediates that allow for lower energy C-C bond breakage than CF_3COO. Among the listed C_2 intermediates, CF_3CFOO requires the lowest energy change for C-C bond breakage. However, it demands a substantial energy increase to form through the CF_3CFO oxygenation reaction. The C-C bond scission of CF_3CF_2O to form CF_3 and CF_2O is highly likely to occur, particularly at the (001) facet. Compared to the CF_3CF_2O defluorination reaction (less than 0 eV at all sites), the CF_3CF_2O defluorination is more probable than C-C scission reaction. The energy change for breaking the C-C bond in CF_3CO is substantially higher than that of CF_3CO oxygenation. Hence, CF_3CO tends to favor the pathway of CF_3COO formation by adding an oxygen atom following the DHEH mechanism, suggesting that the carbon-shortening mechanism of DHEH pathway represents the optimal/main pathway for generating C_1 species from CF_3CF_2.

3.4. Stage III: reaction pathway of C_1 species to CO_2

We discover that all nine possible PFAS-related C_1 intermediates (CF_3, CF_2, CF, CF_3O, CF_2O, CFO, CO, CF_2OO, and CFOO) have viable pathways for mineralization to CO_2 (Fig. 7). Utilizing CF_3 as the probe, the mineralization reaction $CF_3^+ + 2\,H_2O \rightarrow CO_2 + 3HF + H^+$ is represented by a series of oxidation and defluorination reactions. As it is shown in Fig. 7, the first potential path is marked in light blue ($*CF_3 \rightarrow *CF_3O \rightarrow *CF_2O \rightarrow *CFO \rightarrow CO \rightarrow CO_2$), exhibiting the least energy increase for the mineralization of C_1 species to CO_2. Notably, the substances CF and CO have high reactivity towards the lattice oxygen on the surface of β-Ga_2O_3, leading to the formation of CFO (Fig. 7d) and CO_2 (Fig. 7a). Furthermore, at the (001) facet, the intermediate CF_3O undergoes facile adsorption of oxygen and dissociation of fluorine on the catalyst surface, thereby directly generating CF_2O from CF_3 via oxygenation and defluorination.

Given that the transition from CF_3O to CF_2O could occur spontaneously at the (001) site (Fig. 7m), the first potential pathway is the most energetically favorable among all sites (Fig. 8). The pathway reveals that CF_3 undergoes oxygenation and subsequent three-time defluorination, followed by the addition of oxygen to the carbon atom, ultimately leading to the complete mineralization of CF_3.

The second potential pathway, depicted in light red, shares the same $*CF_3 \rightarrow *CF_3O \rightarrow *CF_2O \rightarrow *CFO$ process as the previous pathway. However, $*CFO \rightarrow CO_2$ intermediate in this pathway is CFOO instead of CO. Interestingly, both $*CFO \rightarrow CFOO$ and $*CFO \rightarrow CO$ processes exhibit a negative energy change at all facets, although the latter is deemed more likely to occur. The third potential pathway, shown in gray, proposes that CF_3 can follow the $*CFO \rightarrow CO/CFOO \rightarrow CO_2$ process by initially de-fluorinating to CF_2 and then adding oxygen to form CF_2O. These processes are summarized in Fig. 7(n), where the most favorable pathway ($*CF_3 \rightarrow *CF_3O \rightarrow *CF_2O \rightarrow *CFO \rightarrow CO \rightarrow CO_2$) is an extension of the DHEH pathway to $C_xF_yO_z$ ($x = 1$, $y \leq 3$, $z \leq 1$).

These results indicate that the DHEH pathway offers a viable route for mineralizing long-chain PFAAs to CO_2. At C_1 species to CO_2 stage,

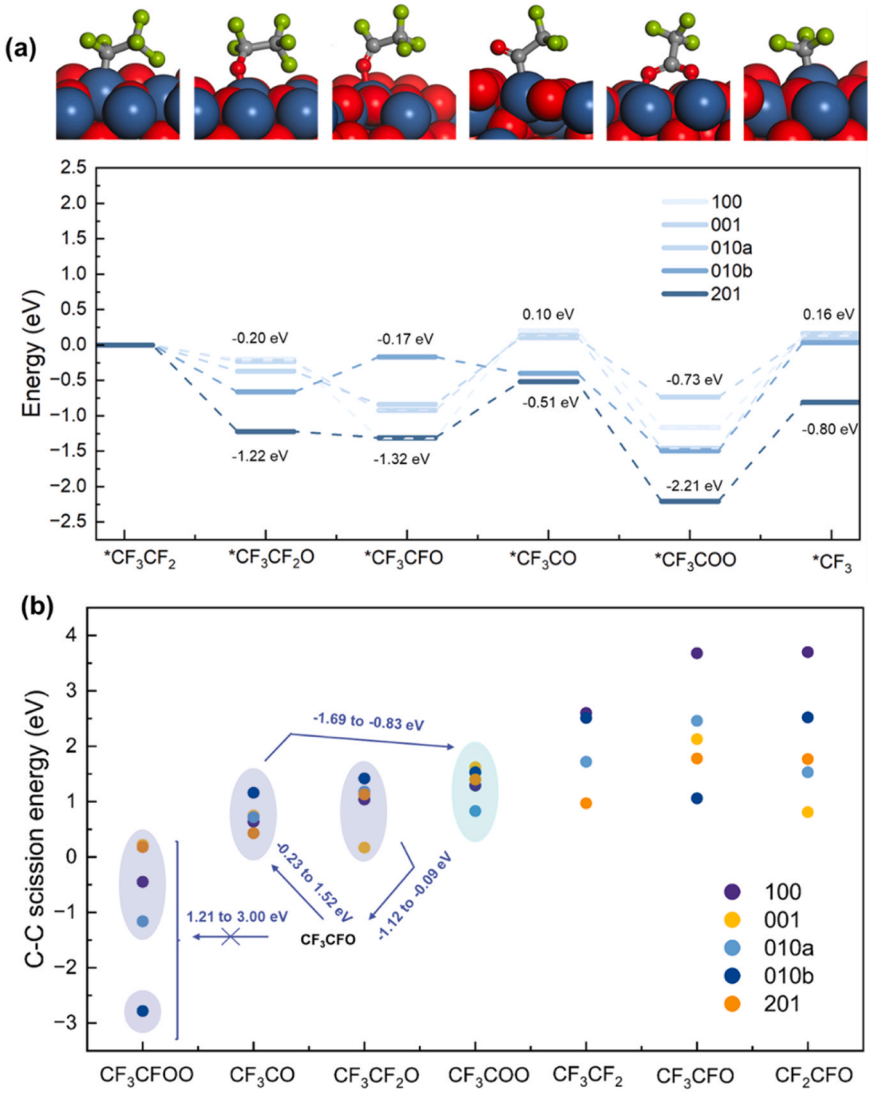

Fig. 6. (a) Energy profiles of pathway II at various β-Ga_2O_3 surfaces, and (b) Site-dependent reaction energy changes in the C-C bond cleavage of various intermediates.

$CF_2O \rightarrow CFO + F$ reaction is energetical among all planes compared to other DHEH mechanism steps. The CFO_2 defluorination energies on the planes follow the order of 100 (1.52 eV) > 010a (0.81 eV) > 201 (0.56 eV) > 001(0.33 eV) > 010b (0.13 eV). Finally, it is worth mentioning that the optimal planes with the highest activity can vary for different reaction stages and intermediates. The 010a site not only demonstrates thermodynamic feasibility for defunctionalization without defluorination in the initial reaction stage, but also exhibits the feasibility of mineralization in C_2 species → C_1 species → CO_2 stages. This observation underscores the advantages of merging the selectivity inherent to material surface active sites with the broad-spectrum degradation capabilities of reactive oxygen species in advanced oxidation processes during PFAS mineralization catalytic reactions.

According to the experimental findings, achieving 100 % defluorination and mineralization through the oxidation of active substances by hydroxyl radicals in various systems (e.g., photochemical/photocatalytic/ electrocatalytic/electron beam) is challenging. Shorter-chain PFCAs products and H/F products fluorotelomer carboxylates (FTCAs, C_nF_{2n+1}–$(CH_2)_m$–COO^-)/sulfonates (FTSAs, C_nF_{2n+1}–$(CH_2)_m$–SO_3^-) have been detected in these systems, suggesting that chain-shortening and H/F exchange are two primary pathways for PFAAs degradation. Mineralization of PFAAs may benefit either chain-shortening or H/F exchange path.

Based on our findings, we propose that mineralization through the DHEH pathway is favorable, while the H/F exchange process can hinder mineralization. The further carbon chain shortening of perfluoroalkyl carbon radicals is associated with generating oxygen-containing products due to the generation of unsaturated coordination through defluorination. The substitution of fluorine with hydrogen atoms will inevitably affect this process. The chemical stability of the produced FTCAs and FTSAs remarkably increases as the H/F exchange proceeds [27,28,57]. Nevertheless, the defluorination reaction is thermodynamically feasible during the initial reaction stages for both PFCAs and PFSAs (Table 1). The C-H bonds formed in the conversion products strengthen the residual C-F bonds, preventing complete defluorination and mineralization. Therefore, the H/F exchange process needs to be controlled. In specific reaction systems, it has been observed that increasing pH and utilizing non-protonic solvents can enhance the defluorination and mineralization rates [27,34].

In photocatalytic degradation systems, besides hydroxyl radicals, many experiments have also indicated that hydrated electrons and holes may play a significant role [25,31,58,59]. According to the experiments and DFT calculations, the hydrate electrons should positively impact PFAS degradation by directly contacting the reactants and intermediates to enhance their defluorination and defunctionalization abilities [25]. This viewpoint is supported by our electronic structure analysis of

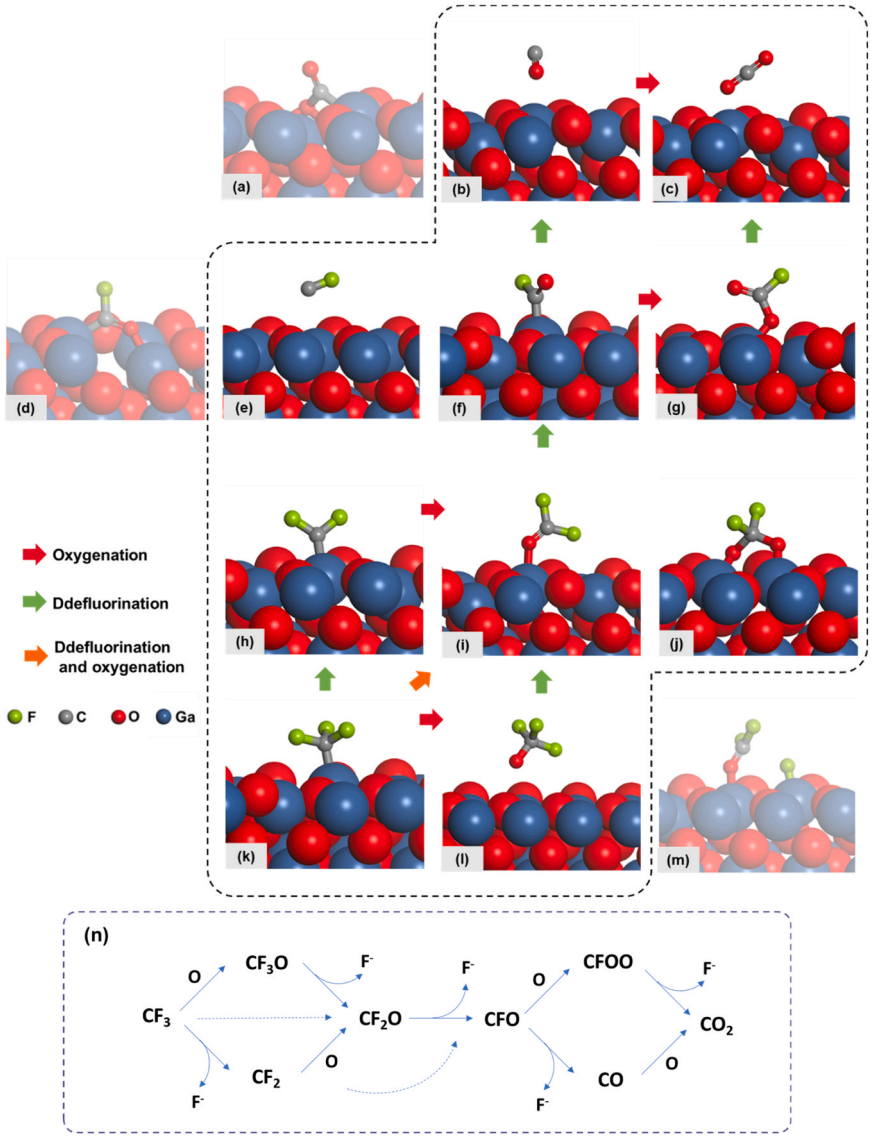

Fig. 7. Models along the reaction pathway for C_1 species on β-Ga_2O_3(001): (a) CO combined with lattice oxygen, (b) CO (gas-phase), (c) CO_2 (gas-phase), (d) CF combined with lattice oxygen, (e) CF (gas-phase), (f) *CFO, (g) *CFOO, (h) *CF_2, (i) *CF_2O, (j) *CF_2OO, (k) *CF_3, (l) *CF_3O, and (m) *CF_2O and *F. The light-colored images represent products rapidly changing from neighboring structures. (n) Proposed mechanism from C_1 species to CO_2.

$C_nF_{2n+1}COO$ with different chain lengths (Fig. S8). The charge density difference results showed similar charge transfer characteristics for PFAS with different chain lengths, with most of the charge accumulation at the carboxyl head and α-positioned F. Combined with the fact that PFAS tends to preferentially undergo the defunctionalization and α-position C defluorination reactions at the initial stage, this suggests that the -COO and -F reactions are related to the obtaining of electrons. The direct interaction of e^-_{aq} with the reactant molecules promotes the electron transfer process of the reactant molecules, thereby facilitating the degradation of PFAS. The holes may play more roles compared to hydroxyl radicals. Because h^+ not only reacts with water to form hydroxyl radicals but also may directly interact with reactants, activating the intermediates or reactants by increasing the initial state (IS) energy and lowering the reaction barrier [58]. In oxides catalytic system, a hole can be captured by lattice oxygen near the reactants, leading to the generation of highly oxidative lattice oxygen radicals ($O^{\bullet-}$) and oxygen vacancies (V_O) [60]. We employed V_O to simulate the reaction in which holes are captured by lattice oxygen in the oxides. Results revealed that the presence of V_O exhibited a higher propensity for the conversion of H_2O to *OH and *OH to *O (Fig. S9) and decreased the energy shift and flattened the energy profile of critical reactions (Fig. S10), making the CF_3COO_2 to CF_3 process more likely to occur.

4. Conclusions

Overall, we have presented the first density functional theory study of systematically investigating the mineralization mechanism of PFCAs (C_3) and PFSAs (C_2) on *β*-Ga_2O_3(100), (001), (010), and (201) facets , including the defluorination and defunctionalization in the initial stage, carbon chain shortening, and mineralization of C_1 species. The results of our simulations provide a computational validation of the extensively proposed DEHE mechanism in advanced oxidation/reduction processes for PFAS treatment, offering quantum-scale details of elementary reactions and the geometric configurations of two ultrashort PFAAs metabolites on material surfaces. Our theoretical results support the following conclusions:

1. We sought the optimal mineralization pathway of two ultrashort PFAAs based on the DHEH mechanism at the quantum scale: CF_3CF_2-R → *CF_3CF_2 → *CF_3CF_2O → *CF_3CFO → *CF_3CO → *CF_3COO → *CF_3 → *CF_3O → *CF_2O → *CFO → *CO → CO_2.

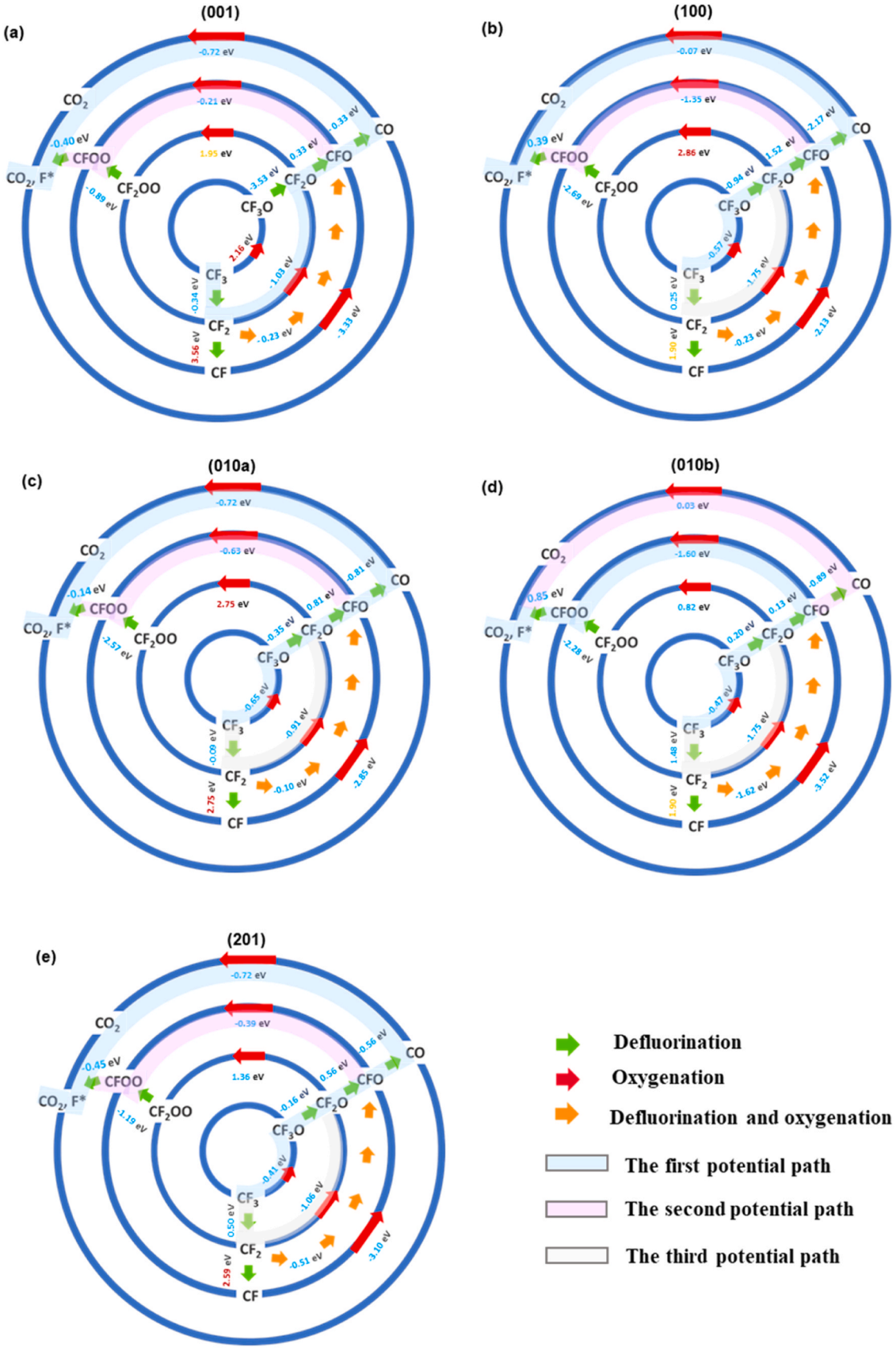

Fig. 8. Mineralization reaction network for C_1 species on: (a) β-Ga_2O_3(001), (b) (100), (c) (010a), (d) (010b), and (e) (201).

2. Our simulations also identified a unique degradation mechanism of PFCAs (C_3) and PFSAs (C_2) on the (010) surface: at the 010a site during the initial reaction stage, only defunctionalization (promoting mineralization) occurs, without defluorination (thus avoiding mineralization hindrance). This emphasizes the combined benefits of site-specific degradation strategies and non-selective approaches involving oxidative radicals to the complete conversion of the parent PFAS to CO_2 and fluorine ions.

3. CF_3COO is identified as the crucial intermediate in the complete mineralization pathway.

These findings contribute to a better understanding of PFAS degradation, and can guide the design of PFAS mineralization catalysts, providing valuable information for developing effective remediation strategies.

CRediT authorship contribution statement

J.W.: Investigation, Conceptualization, Data curation, Formal analysis, Writing – original draft. **Y.M.**: Formal analysis, Writing – review & editing. **S.Y.**: Discussion, Writing – review & editing. **S.R.**: Discussion, Writing – review & editing. **W.G.**: Supervision, Writing – review & editing, Funding acquisition. **Z. W.**: Supervision, Conceptualization, Data curation, Formal analysis, Writing – review & editing.

Declaration of Competing Interest

The authors declare the following financial interests/personal relationships which may be considered as potential competing interests: Ziyun Wang reports financial support was provided by Royal Society of New Zealand. Wei Gao reports financial support was provided by NZ Institute for Minerals to Materials Research. Junyao Wu reports financial support was provided by China Scholarships Council.

Data availability

Data will be made available on request.

Acknowledgments

This work was supported by China Scholarships Council. The project has also partially supported by a joint project (UOA 6000446) of the University of Auckland and NZ Institute for Minerals to Materials Research. ZW wish to acknowledge Marsden Fund Council from Government funding (21-UOA-237) and Catalyst: Seeding General Grant (22-UOA-031-CGS), managed by Royal Society Te Apārangi. All the calculations were performed on the New Zealand eScience Infrastructure (NeSI) high-performance computing facilities.

Appendix A. Supporting information

Supplementary data associated with this article can be found in the online version at doi:10.1016/j.apcatb.2023.123556.

References

[1] L. Jane, L. Espartero, M. Yamada, J. Ford, G. Owens, T. Prow, A. Juhasz, Health-related toxicity of emerging per- and polyfluoroalkyl substances: comparison to legacy PFOS and PFOA, Environ. Res. 212 (2022), 113431.
[2] Z. Wang, A.M. Buser, I.T. Cousins, S. Demattio, W. Drost, O. Johansson, K. Ohno, G. Patlewicz, A.M. Richard, G.W. Walker, G.S. White, E. Leinala, A. New, OECD definition for per- and polyfluoroalkyl substances, Environ. Sci. Technol. 55 (2021) 15575–15578.
[3] S. Kurwadkar, J. Dane, S.R. Kanel, M.N. Nadagouda, R.W. Cawdrey, B. Ambade, G. C. Struckhoff, R. Wilkin, Per- and polyfluoroalkyl substances in water and wastewater: a critical review of their global occurrence and distribution, Sci. Total Environ. 809 (2022), 151003.
[4] S.E. Fenton, A. Ducatman, A. Boobis, J.C. DeWitt, C. Lau, C. Ng, J.S. Smith, S. M. Roberts, Per- and polyfluoroalkyl substance toxicity and human health review: current state of knowledge and strategies for informing future research, Environ. Toxicol. Chem. 40 (2021) 606–630.
[5] S. Rayne, K. Forest, Perfluoroalkyl sulfonic and carboxylic acids: a critical review of physicochemical properties, levels and patterns in waters and wastewaters, and treatment methods, J. Environ. Sci. Health A Toxicol. Hazard. Subst. Environ. Eng. 44 (2009) 1145–1199.
[6] S. Sharma, N.P. Shetti, S. Basu, M.N. Nadagouda, T.M. Aminabhavi, Remediation of per- and polyfluoroalkyls (PFAS) via electrochemical methods, Chem. Eng. J. 430 (2022), 132895.
[7] M. Mirabediny, J. Sun, T.T. Yu, B. Åkermark, B. Das, N. Kumar, Effective PFAS degradation by electrochemical oxidation methods-recent progress and requirement, Chemosphere 321 (2023), 138109.
[8] M. Veciana, J. Bräunig, A. Farhat, M.-L. Pype, S. Freguia, G. Carvalho, J. Keller, P. Ledezma, Electrochemical oxidation processes for PFAS removal from contaminated water and wastewater: fundamentals, gaps and opportunities towards practical implementation, J. Hazard. Mater. 434 (2022), 128886.
[9] R.K. Singh, S. Fernando, S.F. Baygi, N. Multari, S.M. Thagard, T.M. Holsen, Breakdown products from perfluorinated alkyl substances (PFAS) degradation in a plasma-based water treatment process, Environ. Sci. Technol. 53 (2019) 2731–2738.
[10] R.K. Singh, E. Brown, S. Mededovic Thagard, T.M. Holsen, Treatment of PFAS-containing landfill leachate using an enhanced contact plasma reactor, J. Hazard. Mater. 408 (2021), 124452.
[11] J. Wang, Z. Lin, X. He, M. Song, P. Westerhoff, K. Doudrick, D. Hanigan, Critical review of thermal decomposition of per- and polyfluoroalkyl substances: mechanisms and implications for thermal treatment processes, Environ. Sci. Technol. 56 (2022) 5355–5370.
[12] M. Altarawneh, M.H. Almatarneh, B.Z. Dlugogorski, Thermal decomposition of perfluorinated carboxylic acids: kinetic model and theoretical requirements for PFAS incineration, Chemosphere 286 (2022), 131685.
[13] S. Yadav, I. Ibrar, R.A. Al-Juboori, L. Singh, N. Ganbat, T. Kazwini, E. Karbassiyazdi, A.K. Samal, S. Subbiah, A. Altaee, Updated review on emerging technologies for PFAS contaminated water treatment, Chem. Eng. Res. Des. 182 (2022) 667–700.
[14] S.C.E. Leung, P. Shukla, D. Chen, E. Eftekhari, H. An, F. Zare, N. Ghasemi, D. Zhang, N.-T. Nguyen, Q. Li, Emerging technologies for PFOS/PFOA degradation and removal: a review, Sci. Total Environ. 827 (2022), 153669.
[15] F. Liu, X. Guan, F. Xiao, Photodegradation of per- and polyfluoroalkyl substances in water: a review of fundamentals and applications, J. Hazard. Mater. 439 (2022), 129580.
[16] Z. Liu, M.J. Bentel, Y. Yu, C. Ren, J. Gao, V.F. Pulikkal, M. Sun, Y. Men, J. Liu, Near-quantitative defluorination of perfluorinated and fluorotelomer carboxylates and sulfonates with integrated oxidation and reduction, Environ. Sci. Technol. 55 (2021) 7052–7062.
[17] B. Xu, M.B. Ahmed, J.L. Zhou, A. Altaee, M. Wu, G. Xu, Photocatalytic removal of perfluoroalkyl substances from water and wastewater: mechanism, kinetics and controlling factors, Chemosphere 189 (2017) 717–729.
[18] D. Leonello, M.A. Fendrich, F. Parrino, N. Patel, M. Orlandi, A. Miotello, Light-induced advanced oxidation processes as PFAS remediation methods: a review, NATO Adv. Sci. Inst. Ser. E Appl. Sci. 11 (2021) 8458.
[19] L. Duan, B. Wang, K. Heck, S. Guo, C.A. Clark, J. Arredondo, M. Wang, T.P. Senftle, P. Westerhoff, X. Wen, Y. Song, M.S. Wong, Efficient photocatalytic PFOA degradation over boron nitride, Environ. Sci. Technol. Lett. 7 (2020) 613–619.
[20] Y. Wen, Á. Rentería-Gómez, G.S. Day, M.F. Smith, T.-H. Yan, R.O.K. Ozdemir, O. Gutierrez, V.K. Sharma, X. Ma, H.-C. Zhou, Integrated photocatalytic reduction and oxidation of perfluorooctanoic acid by metal-organic frameworks: key insights into the degradation mechanisms, J. Am. Chem. Soc. 144 (2022) 11840–11850.
[21] L. Qian, F.-D. Kopinke, A. Georgi, Photodegradation of perfluorooctanesulfonic acid on Fe-zeolites in water, Environ. Sci. Technol. 55 (2021) 614–622.
[22] W. Wang, Z. Zhou, H. Shao, S. Zhou, G. Yu, S. Deng, Cationic covalent organic framework for efficient removal of PFOA substitutes from aqueous solution, Chem. Eng. J. 412 (2021), 127509.
[23] W. Ji, L. Xiao, Y. Ling, C. Ching, M. Matsumoto, R.P. Bisbey, D.E. Helbling, W. R. Dichtel, Removal of GenX and perfluorinated alkyl substances from water by amine-functionalized covalent organic frameworks, J. Am. Chem. Soc. 140 (2018) 12677–12681.
[24] H. Li, A.L. Junker, J. Wen, L. Ahrens, M. Sillanpää, J. Tian, F. Cui, L. Vergeynst, Z. Wei, A recent overview of per- and polyfluoroalkyl substances (PFAS) removal by functional framework materials, Chem. Eng. J. 452 (2023), 139202.
[25] J. Cui, P. Gao, Y. Deng, Destruction of per- and polyfluoroalkyl substances (PFAS) with advanced reduction processes (ARPs): a critical review, Environ. Sci. Technol. 54 (2020) 3752–3766.
[26] Z. Cheng, Q. Chen, Z. Liu, J. Liu, Y. Liu, S. Liu, X. Gao, Y. Tan, Z. Shen, Interpretation of reductive PFAS defluorination with quantum chemical parameters, Environ. Sci. Technol. Lett. 8 (2021) 645–650.
[27] M.J. Bentel, Z. Liu, Y. Yu, J. Gao, Y. Men, J. Liu, Enhanced degradation of perfluorocarboxylic acids (PFCAs) by UV/sulfite treatment: reaction mechanisms and system efficiencies at pH 12, Environ. Sci. Technol. Lett. 7 (2020) 351–357.
[28] M.J. Bentel, Y. Yu, L. Xu, Z. Li, B.M. Wong, Y. Men, J. Liu, Defluorination of per- and polyfluoroalkyl substances (PFASs) with hydrated electrons: structural dependence and implications to PFAS remediation and management, Environ. Sci. Technol. 53 (2019) 3718–3728.
[29] D.J. Van Hoomissen, S. Vyas, Early events in the reductive dehalogenation of linear perfluoroalkyl substances, Environ. Sci. Technol. Lett. 6 (2019) 365–371.

[30] S. Biswas, S.S.R.K.C. Yamijala, B.M. Wong, Degradation of per- and polyfluoroalkyl substances with hydrated electrons: a new mechanism from first-principles calculations, Environ. Sci. Technol. 56 (2022) 8167–8175.
[31] M. Gar Alalm, D.C. Boffito, Mechanisms and pathways of PFAS degradation by advanced oxidation and reduction processes: a critical review, Chem. Eng. J. 450 (2022), 138352.
[32] Y. Chen, M. Bhati, B.W. Walls, B. Wang, M.S. Wong, T.P. Senftle, Mechanistic insight into the photo-oxidation of perfluorocarboxylic acid over boron nitride, Environ. Sci. Technol. 56 (2022) 8942–8952.
[33] J. Wang, C. Cao, Y. Wang, Y. Wang, B. Sun, L. Zhu, In situ preparation of p-n BiOI@Bi5O7I heterojunction for enhanced PFOA photocatalytic degradation under simulated solar light irradiation, Chem. Eng. J. 391 (2020), 123530, https://doi.org/10.1016/j.cej.2019.123530.
[34] B. Trang, Y. Li, X.-S. Xue, M. Ateia, K.N. Houk, W.R. Dichtel, Low-temperature mineralization of perfluorocarboxylic acids, Science 377 (2022) 839–845.
[35] S. Verma, R.S. Varma, M.N. Nadagouda, Remediation and mineralization processes for per- and polyfluoroalkyl substances (PFAS) in water: a review, Sci. Total Environ. 794 (2021), 148987.
[36] G. Kresse, J. Furthmüller, Efficiency of ab-initio total energy calculations for metals and semiconductors using a plane-wave basis set, Comput. Mater. Sci. 6 (1996) 15–50.
[37] G. Kresse, J. Furthmüller, Efficient iterative schemes for ab initio total-energy calculations using a plane-wave basis set, Phys. Rev. B Condens. Matter 54 (1996) 11169–11186.
[38] G. Kresse, D. Joubert, From ultrasoft pseudopotentials to the projector augmented-wave method, Phys. Rev. B Condens. Matter 59 (1999) 1758–1775.
[39] P.E. Blöchl, O. Jepsen, O.K. Andersen, Improved tetrahedron method for Brillouin-zone integrations, Phys. Rev. B Condens. Matter 49 (1994) 16223–16233.
[40] H.J. Monkhorst, J.D. Pack, Special points for Brillouin-zone integrations, Phys. Rev. B Condens. Matter 13 (1976) 5188–5192.
[41] W. Zhang, D. Zhang, Y. Liang, Nanotechnology in remediation of water contaminated by poly- and perfluoroalkyl substances: a review, Environ. Pollut. 247 (2019) 266–276.
[42] S. Yoshioka, H. Hayashi, A. Kuwabara, F. Oba, K. Matsunaga, I. Tanaka, Structures and energetics of Ga2O3 polymorphs, J. Phys. Condens. Matter 19 (2007), 346211.
[43] B. Anam, N. Gaston, Structural, thermal, and electronic properties of two-dimensional gallium oxide(ß-Ga2O3) from first-principles design, Chemphyschem 22 (2021) 2362–2370.
[44] Y. Wen, Á. Rentería-Gómez, G.S. Day, M.F. Smith, T.-H. Yan, R.O.K. Ozdemir, O. Gutierrez, V.K. Sharma, X. Ma, H.-C. Zhou, Integrated photocatalytic reduction and oxidation of perfluorooctanoic acid by metal–organic frameworks: key insights into the degradation mechanisms, J. Am. Chem. Soc. 144 (2022) 11840–11850.
[45] Z. Wang, Y. Li, J. Boes, Y. Wang, E. Sargent, CO_2 electrocatalyst design using graph theory, Res. Sq. (2020), https://doi.org/10.21203/rs.3.rs-66715/v1.
[46] R.C. Buck, J. Franklin, U. Berger, J.M. Conder, I.T. Cousins, P. de Voogt, A. A. Jensen, K. Kannan, S.A. Mabury, S.P.J. van Leeuwen, Perfluoroalkyl and polyfluoroalkyl substances in the environment: terminology, classification, and origins, Integr. Environ. Assess. Manag. 7 (2011) 513–541.
[47] S. Rayne, K. Forest, An assessment of organic solvent based equilibrium partitioning methods for predicting the bioconcentration behavior of perfluorinated sulfonic acids, carboxylic acids, and sulfonamides, Nat. Preced. (2009) 1–2.
[48] C.J. Liu, G. McKay, D. Jiang, R. Tenorio, J.T. Cath, C. Amador, C.C. Murray, J. B. Brown, H.B. Wright, C. Schaefer, C.P. Higgins, C. Bellona, T.J. Strathmann, Pilot-scale field demonstration of a hybrid nanofiltration and UV-sulfite treatment train for groundwater contaminated by per- and polyfluoroalkyl substances (PFASs), Water Res. 205 (2021), 117677.
[49] R. Tenorio, J. Liu, X. Xiao, A. Maizel, C.P. Higgins, C.E. Schaefer, T.J. Strathmann, Destruction of per- and polyfluoroalkyl substances (PFASs) in aqueous film-forming foam (AFFF) with UV-sulfite photoreductive treatment, Environ. Sci. Technol. 54 (2020) 6957–6967.
[50] X. Dai, Z. Xie, B. Dorian, S. Gray, J. Zhang, Comparative study of PFAS treatment by UV, UV/ozone, and fractionations with air and ozonated air, Environ. Sci.: Water Res. Technol. 5 (2019) 1897–1907.
[51] N. Chowdhury, S. Prabakar, H. Choi, Dependency of the photocatalytic and photochemical decomposition of per-and polyfluoroalkyl substances (PFAS) on their chain lengths, functional groups, and structural properties, Water Sci. Technol. 84 (2021) 3738–3754.
[52] H. Cao, J. Peng, Z. Zhou, Y. Sun, Y. Wang, Y. Liang, Insight into the defluorination ability of per- and polyfluoroalkyl substances based on machine learning and quantum chemical computations, Sci. Total Environ. (2021), 151018.
[53] M.J. Bentel, Y. Yu, L. Xu, H. Kwon, Z. Li, B.M. Wong, Y. Men, J. Liu, Degradation of perfluoroalkyl ether carboxylic acids with hydrated electrons: structure–reactivity relationships and environmental implications, Environ. Sci. Technol. 54 (2020) 2489–2499.
[54] Y. Zhu, H. Ji, K. He, L. Blaney, T. Xu, D. Zhao, Photocatalytic degradation of GenX in water using a new adsorptive photocatalyst, Water Res. 220 (2022), 118650.
[55] E. Banayan Esfahani, F. Asadi Zeidabadi, S. Zhang, M. Mohseni, Photo-chemical/catalytic oxidative/reductive decomposition of per- and poly-fluoroalkyl substances (PFAS), decomposition mechanisms and effects of key factors: a review, Environ. Sci. 8 (2022) 698–728.
[56] J. Niu, H. Lin, C. Gong, X. Sun, Theoretical and experimental insights into the electrochemical mineralization mechanism of perfluorooctanoic acid, Environ. Sci. Technol. 47 (2013) 14341–14349.
[57] L. Liu, S. Deng, Y. Bao, J. Huang, G. Yu, Degradation of OBS (sodium p-perfluorous nonenoxybenzenesulfonate) as a novel per- and polyfluoroalkyl substance by UV/persulfate and UV/sulfite: Fluorinated intermediates and treatability in fluoroprotein foam, Environ. Sci. Technol. 56 (2022) 6201–6211.
[58] Y. Sun, G. Li, W. Wang, W. Gu, P.K. Wong, T. An, Photocatalytic defluorination of perfluorooctanoic acid by surface defective BiOCl: fast microwave solvothermal synthesis and photocatalytic mechanisms, J. Environ. Sci. (China) 84 (2019) 69–79.
[59] W. Wang, Y. Chen, G. Li, W. Gu, T. An, Photocatalytic reductive defluorination of perfluorooctanoic acid in water under visible light irradiation: the role of electron donor, Environ. Sci.: Water Res. Technol. 6 (2020) 1638–1648.
[60] J. Zhang, C. Peng, H. Wang, P. Hu, Identifying the role of photogenerated holes in photocatalytic methanol dissociation on rutile TiO_2(110), ACS Catal. 7 (2017) 2374–2380.